

Date 2010
Author Besten, H.J. den and R.H.M. Huijsmans.

Address Delft University of Technology
Ship Hydromechanics Laboratory
Mekelweg 2, 2628 CD Delft



Delft University of Technology

**Fatigue in High-Speed Ships: Crack Propagation
in Aluminium**

by

H.J. den Besten and R.H.M. Huijsmans

Report No. 1698-P

2010

**Published in: Proceedings of the 11th International
Symposium on Practical Design of Ships and Other
Floating Structures, Rio de Janeiro, Brazil**

Fatigue in High-Speed Ships: Crack Propagation in Aluminum

J.H. den Besten ¹⁾, R.H.M. Huijsmans ¹⁾

¹⁾ Ship Hydromechanics & Structures, Delft University of Technology
Delft, The Netherlands

Abstract

To develop a design method concerning high-cycle fatigue of arc-welded joints in high-speed aluminum ships, two-stage crack growth, micro-crack and macro-crack growth, propagation, in aluminum 5083 has been investigated using a Linear Elastic Fracture Mechanics (LEFM) approach. The macro-crack growth governing LEFM parameter, the Stress Intensity Factor (SIF), is obtained using available handbook solutions. This SIF is corrected using the Stress Concentration Factor (SCF) related analytical, parametric notch stress formulations of the uncracked geometry of the welded joints, applied as crack face pressure, to cover micro-crack growth. The notch stress formulations and SIF's for some basic welded joints are compared to Finite Element (FE) solutions and match quite well. The two-stage crack growth model is compared to experimental data of a Single Edge Notch (SEN) specimen and show promising results.

Keywords

High-cycle fatigue; aluminum 5083; arc-welded joints; crack growth.

Introduction

For many years, aluminum alloys have become the standard for high-speed ships. An important reason is the good welding characteristics, since arc-welding is the primary method for joining ship structure components. However, it is well-known that arc-

welded joints may exhibit poor fatigue properties. Besides, aluminum alloys generally have higher crack propagation rates and smaller (fracture) toughness compared to steel. Because of the dynamic loading of high-speed ships, fatigue is a governing failure mechanism and welded aluminum joints are in terms of fatigue often the most critical parts of the ship structure.

To develop a design method for (high cycle) fatigue of high-speed aluminum ships, the maritime innovation project "VOMAS" has been initiated. Part of the scope is developing a fatigue master curve approach for arc-welded aluminum joints. It is inspired by the impressive work of (Atzori, 1997, 2005 and Lazzarin et al., 1996) and (Dong et al., 2001, 2003a, 2003b). Some research results are described in this paper.

Fatigue is the progressive and (extremely) localized structural damage that may occur when a structure is subjected to cyclic loading. It is concerned with crack initiation and crack growth, crack propagation, as shown in (Fig. 1).

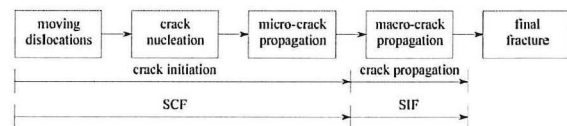


Fig. 1: Fatigue Fracture Scheme (Schijve, 2001)

Crack initiation is a surface phenomenon; governing parameter is the Stress Concentration Factor (SCF). Micro-crack growth is included in this period because of the low crack growth rate. When the crack penetrates into the material, the material bulk

property induced macro-crack growth resistance controls the crack growth rate. Governing parameter in this crack propagation period is the Stress Intensity Factor (SIF). Both parameters are geometry and load distribution determined.

High-speed ship structures experience a large number of cycles N during its lifetime; operate in the high-cycle fatigue region. It is assumed that crack propagation dominates, since it is inevitable that flaws, crack nuclei, already exist because of arc-welding as joining method. Hence, the Linear Elastic Fracture Mechanics (LEFM) principles are adopted.

However, crack propagation consists of micro-crack growth and macro-crack growth. Both stages are considered to be important. Micro-crack growth in particular since a significant part of the fatigue life may be consumed in this stage, because of the low crack growth rate. Hence, the macro-crack growth governing LEFM parameter, the SIF K , will be corrected for micro-crack growth using the SCF related notch stress distribution.

In this paper, structural stress based notch stress distributions will be determined for some basic welded joints. Subsequently, the SIF's will be determined; to be used in a Paris based two-stage crack growth equation. This model will be verified using experimental crack growth data of aluminum 5083-H321 specimens.

Weld Notch Stress Distributions

The aim is to develop analytical, parametric notch stress formulations – with its characteristic singularity – for basic welded joints, which account for all involved geometry parameters. It will be related to a linear far field stress distribution, obtained in a Finite Element (FE) environment with shell elements.

The notch stress distribution is assumed to be a superposition of a non-linear notch stress part – Williams' asymptotic solution – and a linear weld geometry induced bending part (together the self-equilibrating stress part) and the linear far field stress (equilibrium equivalent stress part), as shown in (Fig. 2) for a Full Penetration (FP), Double Sided (DS) T-joint. Monotonic as well as non-monotonic notch stress distributions will be considered.

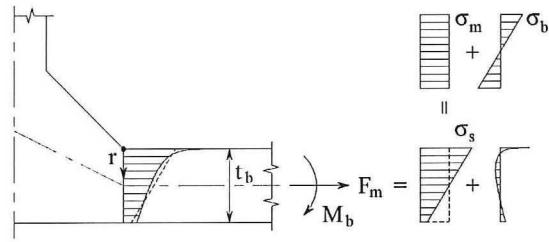


Fig 2: Weld Notch Stress Distribution

The far field stress distribution is the linear stress distribution in the cross-section at the weld toe (weld toe failure) or weld root (weld root failure), as already introduced by (Niemi et al., 2004). It is consistent with the far field stress definition in the fracture mechanics context. For shell plated (ship) structures, the loading is predominantly membrane and bending induced. The nodal forces can be used to obtain the corresponding membrane and bending stress amplitudes, σ_m and σ_b :

$$\sigma_m = \frac{F_m}{t_b} \quad (1)$$

$$\sigma_b = 6 \cdot \frac{M_b}{t_b^2} \quad (2)$$

The far field stress distribution will be characterized by two parameters, the structural stress amplitude σ_s , which is the stress amplitude at the notch and the bending stress ratio R .

The structural stress amplitude σ_s is determined by the sign of the membrane force $\text{sgn}(F_m)$ and bending moment $\text{sgn}(M_b)$ and the corresponding stress amplitudes, σ_m and σ_b respectively, as shown in (Eq. 3).

$$\sigma_s = \text{sgn}(F_m) \cdot \sigma_m - \text{sgn}(M_b) \cdot \sigma_b \quad (3)$$

The minus sign in (Eq. 3) is a result of the used coordinate system: counterclockwise positive. The bending stress ratio R describes the amount of bending relative to the structural stress and the sign of the slope of the far field stress distribution:

$$R = \text{sgn}(M_b) \cdot \frac{\sigma_b}{\sigma_s} \quad (4)$$

A positive R indicates that the notch stress distribution will be non-monotonic; a negative R a monotonic notch stress distribution.

As already shown in (Fig. 2), the weld geometry introduces a change of stiffness, a shift in neutral axis, inducing a counter clockwise bending moment, a weld geometry induced bending stress (σ_{bm} and σ_{bb} for membrane force and bending moment respectively). Note that this stress component is not part of the equilibrating far field stress. The weld geometry induced bending part formulates together with Williams' asymptotic solution the self equilibrating stress part. It is related to the far field stress using the constants C_{bm} and C_{bb} :

$$\sigma_{bm} = C_{bm} \cdot \sigma_m \quad (5)$$

$$\sigma_{bb} = C_{bb} \cdot \sigma_b \quad (6)$$

A superposition of (Eqs. 5~6) comprises the total amount of weld geometry induced bending, (Eq. 7), which has been related to σ_s .

$$C_{gb} = \text{sgn}(F_m) \cdot C_{bm} + R \cdot \{ \text{sgn}(F_m) \cdot C_{bm} + \text{sgn}(M_b) \cdot C_{bb} \} \quad (7)$$

The authors have to admit that it is not that easy to determine C_{gb} , but using a beam FE model, quite satisfying results have been obtained. An example is shown in (Fig. 3) for the FP DS T-joint. The striped lines represent rigid connections.

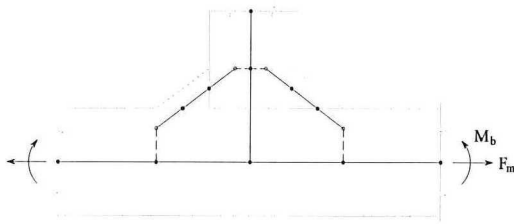


Fig. 3: FE beam model for FP DS T-joint

For Williams' asymptotic solution, the normal stress component σ_{00} with a particular stress angle β has been used (Williams, 1952). The symmetric and anti-symmetric parameters λ_s and λ_a are the eigenvalues; χ_s and χ_a the corresponding eigenvalue coefficients.

The two coefficients μ_s and μ_a that have to be solved for require boundary conditions, which are different for welded joints with non-symmetry or symmetry with respect to half the base plate thickness.

Non-Symmetric Joint

Examples of basic types of welded joints which are non-symmetric with respect to $(t_b/2)$ are: FP DS T-joints, Load Carrying (LC) cruciform joints, Single Side (SS) cover plates and knee connections. The weld notch stress distribution is described by (Eq. 8).

$$\frac{\sigma_w \left(\frac{r}{t_b} \right)}{\sigma_s} = \quad (8)$$

$$\mu_s \cdot \lambda_s \cdot (\lambda_s + 1) \cdot$$

$$[\cos\{(\lambda_s + 1) \cdot \beta\} - \chi_s \cdot \cos\{(\lambda_s - 1) \cdot \beta\}] \cdot \left(\frac{r}{t_b} \right)^{\lambda_s - 1} +$$

$$\mu_a \cdot \lambda_a \cdot (\lambda_a + 1) \cdot$$

$$[\sin\{(\lambda_a + 1) \cdot \beta\} - \chi_a \cdot \sin\{(\lambda_a - 1) \cdot \beta\}] \cdot \left(\frac{r}{t_b} \right)^{\lambda_a - 1} +$$

$$C_{gb} \cdot \left\{ 2 \cdot \left(\frac{r}{t_b} \right) - 1 \right\} + 2 \cdot R \cdot \left(\frac{r}{t_b} \right)$$

Williams' asymptotic solution, the weld geometry induced bending part and the far field bending stress projection can be clearly distinguished. It is rather straight forward to use force and moment equilibrium to solve for μ_s and μ_a in (Eq. 8). Two examples are shown in (Figs. 4~5) for a FP DS T-joint for a monotonic and non-monotonic case. Notch radius effects (ρ/t_b) are not taken into account. The obtained analytical formulation and FE results match quite well.

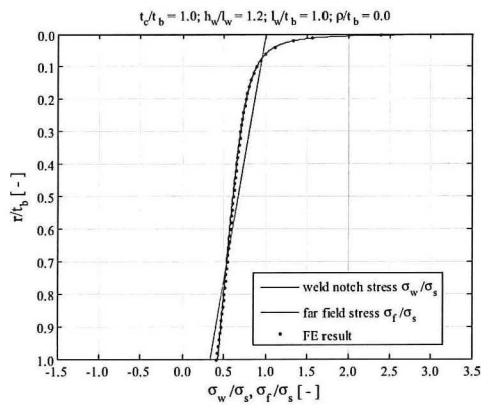


Fig. 4: Notch Stress Distr. DS FP T-joint (monotonic)

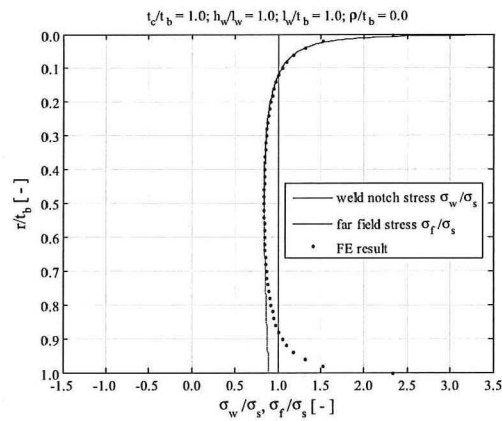


Fig. 6: Notch Stress Distr. FP Cr. Joint (monotonic)

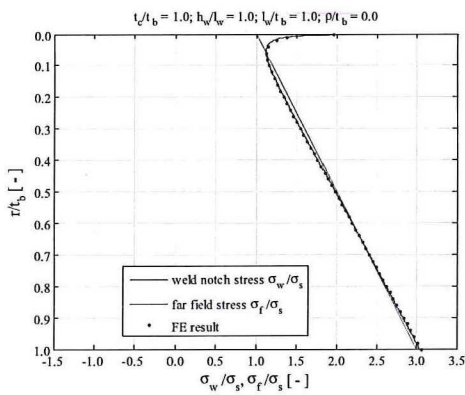


Fig. 5: Notch Stress Distr. DS FP T-joint (non-monotonic)

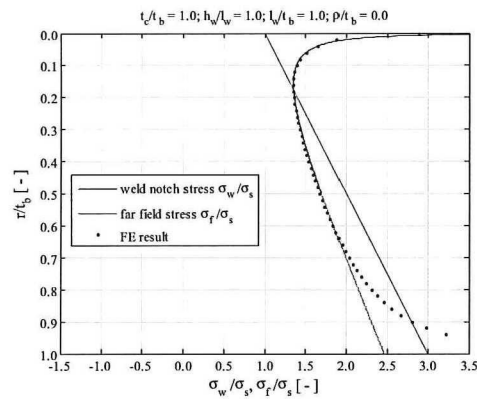


Fig. 7: Notch Stress Distr. FP Cr Joint (non-monotonic)

Symmetric Joint

Examples of basic types of welded joints which are symmetric with respect to $(t_b/2)$ are FP cruciform joints and FP DS butt joints. Because of symmetry, only half the base plate thickness t_b will be considered. Using force and moment equilibrium is not sufficient because of symmetry conditions at $(r/t_b) = 1/2$. Hence, it is decided to satisfy force equilibrium and $d\sigma_w \{(r/t_b) = 1/2\} / dr = 0$. The latter condition is chosen to satisfy symmetry prior to moment equilibrium; an anti-symmetric stress distribution is covered by the far field bending stress projection. If accurate weld notch stress distributions are obtained, moment equilibrium is identically satisfied.

Two examples are shown in (Figs. 6~7) for a FP Cruciform-joint, a monotonic and non-monotonic case. Note that the notch effects in the symmetry part are ignored since it is considered only to be important for micro-crack growth, short crack growth. The analytical formulations seem to be a sound basis to define a correction factor for the SIF, to cover micro-crack growth.

Stress Intensity Factors

Generalized K solutions for welded joints are not available. Fortunately, the equilibrium equivalent stress part of the weld notch stress distribution is consistent with the far field stress definition in fracture mechanics. As a result, for any crack size along the weld, K will be estimated by superposition of the existing K solutions for simple fracture mechanics specimen, subjected to membrane and bending loading, considering either an edge crack (two-dimensional) or a semi-elliptical crack (three-dimensional). The self-equilibrating stress part is consistent with the crack face pressure definition in fracture mechanics and will be translated to its contribution, correction, to K.

With respect to the different crack modes, the crack opening mode, mode I, is considered to be dominant for shell plated (ship) structures, since the base plate thickness t_b is the critical parameter: $t_b \ll$ plate length and plate width and the loading is predominantly membrane and bending induced. The tearing mode,

mode III, which can be important at locations of high in-plane shear stresses, will be ignored for now.

Using LEFM, it is found convenient to write the solution for the SIF of a crack at the weld as a product of crack size dependent correction factors Y_m and Y_g and the SIF for the basic case (Albrecht et al., 1977). The basic case for mode I is a crack with length $2a$ in an infinite plate subjected to a uniform far field stress σ .

$$K_I = Y_m \cdot Y_g \cdot \sigma \cdot \sqrt{\pi \cdot a} \quad (9)$$

The correction factor Y_g accounts for the geometry and far field loading effects; Y_m for the magnification effects as a result of the crack face pressure.

The geometry factor Y_g accounts with respect to the type of far field stress for the finite thickness effects in case of a centre cracked plate (weld root failure) and for the combined free surface and finite thickness effects in case of an edge crack (weld toe failure). Recalling that the far field stress consists of a membrane force and bending moment and using the linear superposition principle, (Eq. 9) becomes:

$$K_I = Y_m \cdot [\text{sgn}(F_m) \cdot Y_{gm} + \quad (10)$$

$$R \cdot \{\text{sgn}(F_m) \cdot Y_{gm} + \text{sgn}(M_b) \cdot Y_{gb}\}] \cdot \sigma_s \cdot \sqrt{\pi \cdot a}$$

The geometry factors Y_{gm} and Y_{gb} are handbook solutions, obtained for edge crack, centre crack and semi-elliptical crack formulations, membrane force and bending moment loaded respectively, using (Tada et al., 2000; Murakami, 1987; Newman et al., 1981).

The correction factor or magnification factor Y_m accounts for the crack face pressure, the non-linear stress along the crack path, $\sigma(x)$, which is the self-equilibrating stress part (of the uncracked geometry) to cover micro-crack growth. The corresponding mode I SIF can be obtained using the well-known SIF of a symmetric line loaded centre crack:

$$Y_m = \left(\frac{2}{\pi}\right) \cdot \int_0^a \frac{\sigma(r)}{\sqrt{a^2 - r^2}} dr \quad (11)$$

Note that $\sigma(r)$ in (Eq. 11) represent the unit stress distribution (σ_w/σ_s), described by (Eq. 8).

The SIF's for two basic types of joints, the FP DS T-joint and the FP cruciform joint, which cover the non-symmetric and symmetric welded joints are determined and compared with FE solutions available from (Smith, 1984).

Y_g , Y_m and $Y_m \cdot Y_g$ for a FP DS T-joint, membrane force loaded, in an edge crack configuration are shown in (Fig. 8). Note the non-monotonic behavior for $Y_m \cdot Y_g$. The magnification factor Y_m dominates for $\{(a/t_b) \leq 0.1\}$ and is concerned with micro-crack growth; the geometry factor Y_g dominates for $\{(a/t_b) > 0.1\}$ and covers macro-crack growth. The region $\{0.1 < (a/t_b) \leq 0.2\}$ is dominated by the weld geometry induced bending.

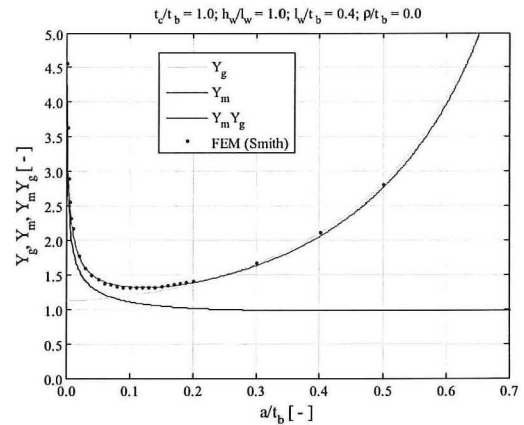


Fig. 8: FP DS T-joint SIF Correction Factors, F_m loaded

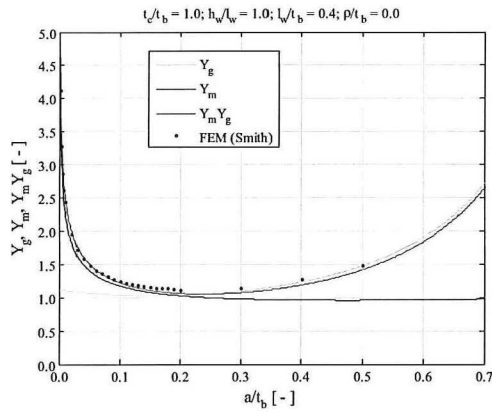


Fig. 9: FP DS T-joint SIF Correction Factors, M_b loaded

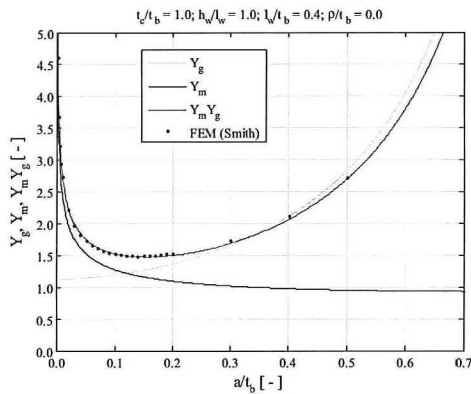


Fig. 10: FP Cr. Joint SIF Correction Factors, F_m loaded

The SIF for the bending moment loaded FP DS T-joint is shown in (Fig. 9). Comparing to the membrane loaded case, the behavior close to the singularity is similar: the weld angle is similar. For increasing (a/t_b) up to $\{(a/t_b) \approx 0.2\}$, the SIF in the bending case becomes somewhat lower as a result of less weld geometry induced bending. In the macro-crack growth region, the difference is quite large in favor of the bending case as a result of the stress gradient.

The edge crack FP Cruciform Joint solutions are shown in (Figs. 10~11). Remember that the symmetry part is ignored, as explained before.

It turns out that the major difference between the T-joint and Cruciform joints occur in the weld geometry induced bending dominating region: $\{0.1 < (a/t_b) \leq 0.2\}$. The notch effects are similar since the weld geometry is similar. In the macro-crack growth region, $\{(a/t_b) > 0.1\}$, the behavior is more or less similar as well: in both cases, edge cracks are considered.

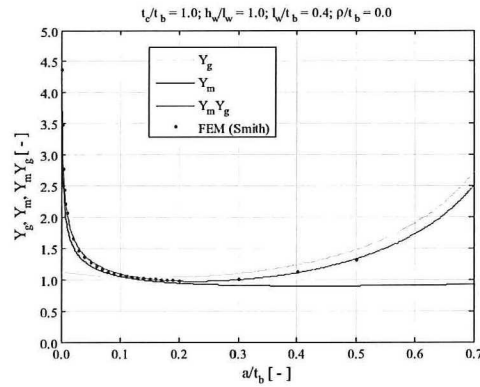


Fig. 11: FP Cr. Joint SIF Correction Factors, M_b loaded

Crack Propagation

A cyclic loading introduces a cyclic stress intensity ΔK and may initiate crack growth, crack propagation. The well-known characteristic crack growth rate curve, $(da/dn) - \Delta K$, with n the number of cycles, shown in (Fig. 12), is divided into three regions; region I (near-threshold, slow crack growth region; below the threshold value ΔK_{th} crack growth does not occur), region II (linear, steady state region) and region III (unstable crack growth region, up to final fracture).

Because of the (very) high crack propagation rate in region III, the number of cycles consumed in this region is quite small and it needs not to be said that this region is not that important from fatigue (design) point of view. Region I is considered to be very important, since a significant part of the fatigue life of welded joints is spent in region I, the micro-crack growth region, because of the low crack growth rate. Hence, a well-known two-stage crack growth model is introduced:

$$\frac{da}{dn} = C \cdot \left\{ 1 - \left(\frac{\Delta K_{th}}{\Delta K} \right) \right\}^n \cdot (\Delta K)^m \quad (12)$$

For micro-crack growth, the (notch) stress related Stress Concentration Factor (SCF) is the governing parameter, as already shown in Fig. 1. For the adopted LEFM approach, the notch stress distribution of the uncracked geometry is included as crack face pressure, which has been found dominating the micro-crack (growth) region, region I, by means of the magnification factor Y_m .

Hence, the region I factor $\{1 - (\Delta K_{th}/\Delta K)\}^n$ in (Eq. 12), which shows similar behavior, is proposed to be replaced by Y_m :

$$\frac{da}{dn} = C \cdot Y_m^n \cdot (\Delta K_g)^m \quad (13)$$

Note that Y_m represents the quotient $\{(\Delta K \text{ with notch effects}) / (\Delta K \text{ without notch effects})\}$ as well. This definition is similar to the one of (Dong, 2003b). The subscript g in ΔK_g is the linear, far field stress induced SIF part (Y_g related) that governs macro-crack growth, region II. This two-stage crack growth will be investigated for the Single Edge Notch (SEN) specimen.

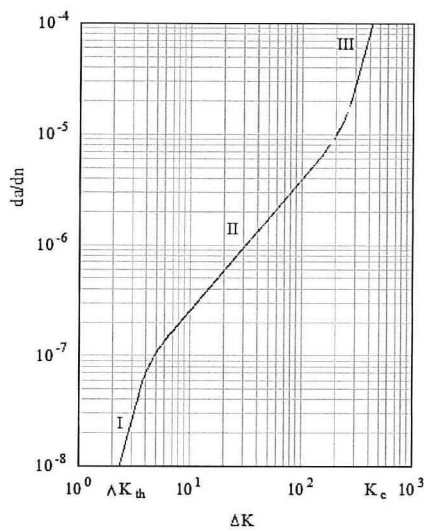


Fig. 12: characteristic crack growth rate curve

Single Edge Notch (SEN) Specimen – Analysis

The membrane force loaded SEN specimen is investigated, as shown in (Fig. 13).

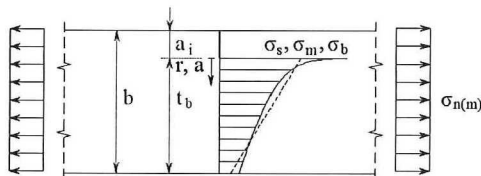


Fig. 13: SEN Specimen

A solution for K of this specimen is directly available from handbook solutions. However, the approach between the crack growth specimens and welded joints has to be consistent. The SIF for the SEN

specimen has been redefined in terms of the (far field) stress components in the cross-section of the crack as shown in (Fig. 13), similar as for the considered welded joints, using the crack face pressure definition (Eq. 11). Note the shift in coordinate system. Micro-crack growth effects are incorporated using the crack notch stress distribution. Results are translated to the two-stage crack growth model and validated using $(da/dn) - \Delta K$ experimental data of aluminum specimens.

In analogy to the previously described procedure, the (monotonic) notch stress distribution at the cross-section of the crack is obtained. The (far field) stress components σ_m , σ_b and σ_s and R are defined in the cross-section of the crack, similar to the welded joints, opposite to the handbook solutions, and related to the nominal (membrane) stress $\sigma_{n(m)}$; the far field stress definition of the handbook solutions. Note that the introduction of the nominal stress is a result of the consideration of a cracked geometry here. The membrane stress amplitude σ_m and the bending stress amplitude σ_b are related to $\sigma_{n(m)}$ using equilibrium conditions:

$$\sigma_m = \sigma_{n(m)} \cdot \frac{1}{\left\{ 1 - \left(\frac{a_i}{b} \right) \right\}} \quad (14)$$

$$\sigma_b = \sigma_{n(m)} \cdot \frac{3 \cdot \left(\frac{a_i}{b} \right)}{\left\{ 1 - \left(\frac{a_i}{b} \right) \right\}^2} \quad (15)$$

Solving the eigenvalue problem that corresponds to Williams' asymptotic solution for $2 \cdot \alpha = 2\pi$, the crack configuration, it turns out that $\lambda_s = \lambda_a = \lambda$ and multiple feasible solutions are found.

$$\lambda_i = \left(\frac{1}{2} \right), \left(\frac{3}{2} \right), \left(\frac{5}{2} \right), \left(\frac{7}{2} \right), \dots$$

Note that only the first eigenvalue $\lambda_1 = (1/2)$ introduces singular behavior of the crack notch stress distribution. Because of the multiplicity of solutions, some engineering judgement has been introduced to determine how many terms and in particular which ones are required to obtain reasonably accurate crack notch stress distributions. Comparing the analytical formulations to FE results showed that three terms are required: the first (singular) one, $\lambda_1 = (1/2)$, and the

second and fourth (non-singular) terms, $\lambda_2 = (3/2)$, $\lambda_4 = (7/2)$. The choice of the different non-singular terms is based on the amount of bending stress and may be different for other loading conditions (bending) and crack growth specimens. The crack notch stress distribution $\sigma_c(r/t_b)$ becomes for $\beta = 0$:

$$\frac{\sigma_c\left(\frac{r}{t_b}\right)}{\sigma_s} = \sum_{i=1,2,4} \left\{ \mu_i \cdot \lambda_i \cdot (\lambda_i + 1) \cdot (1 - \chi_i) \cdot \left(\frac{r}{t_b}\right)^{\lambda_i - 1} \right\} \quad (16)$$

The coefficients μ_i have been solved for using equilibrium and an additional, artificial, relation is required: a relation between the equilibrium coefficients of the non-singular terms μ_2 and μ_4 has been found convenient. An example of a crack notch stress distribution of a SEN specimen is shown in (Fig. 14).

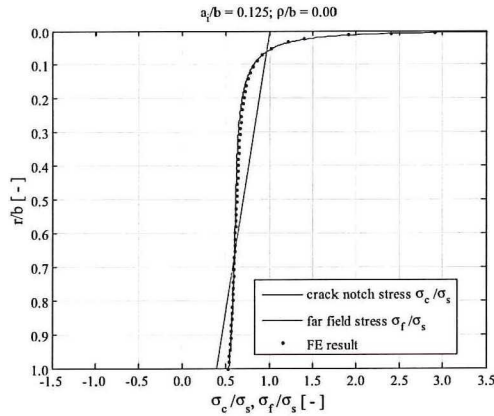


Fig. 14: SEN Specimen Crack Notch Stress Distribution

The SIF handbook solution for the membrane force loaded SEN specimen, including correction for its relation to the linear (far field) stress distribution in the cross-section of the crack and treating the notch as part of the crack length denotes:

$$K_I = Y_1 \cdot Y_{gm} \cdot \sigma_s \cdot \sqrt{\pi \cdot b} \cdot \sqrt{\left(\frac{a_i}{b}\right) + \left(\frac{t_b}{b}\right) \cdot \left(\frac{a}{t_b}\right)} \quad (17)$$

With:

$$Y_1\left(\frac{a}{t_b}\right) = \left(\frac{2}{\pi}\right) \cdot \left(\frac{a_i + a}{t_b}\right) \cdot \left\{ 1 + 2 \cdot R \cdot \left(\frac{r - a_i}{t_b}\right) \right\} \cdot \left(\frac{r}{t_b}\right) \cdot \sqrt{\left(\frac{a_i + a}{t_b}\right)^2 - \left(\frac{r}{t_b}\right)^2}$$

The factor Y_1 corrects for the relation to the linear crack notch stress distribution, using the crack face pressure formulation (Eq. 11). The geometry correction factor Y_{gm} have to be modified because of the shifted coordinate system: replace (a/t_b) by $\{(a_i/b) + (t_b/b) \cdot (a/t_b)\}$.

So far, the micro-crack growth dominating self-equilibrating stress has not been taken into account. It can be introduced by replacing Y_1 by Y_n , obtained in a similar way as Y_1 using the non-linear crack notch stress distribution (Eq. 16). Finally, the two-stage crack growth model for the SEN specimen can be obtained:

$$\frac{da}{dn} = C \cdot \left(\frac{Y_n}{Y_1}\right)^n \quad (18)$$

$$\left\{ Y_1 \cdot Y_{gm} \cdot \Delta\sigma_s \cdot \sqrt{\pi \cdot b} \cdot \sqrt{\left(\frac{a_i}{b}\right) + \left(\frac{t_b}{b}\right) \cdot \left(\frac{a}{t_b}\right)} \right\}^m$$

Note that micro-crack growth effects are included using the quotient $\{(\Delta K \text{ with notch effects}) / (\Delta K \text{ without notch effects})\}$.

SEN Specimen – Experimental Data

Crack growth data for aluminum 5083-H321 SEN specimens in L-T configuration (crack growth perpendicular to rolling direction), published by (Shankar et al., 2002), has been used to validate the two-stage crack growth model. Three data sets were provided, including crack growth in plain material and crack growth in the Heat Affected Zone (HAZ) at the weld toe of DS FP butt weld joints in welding direction and in counter welding direction. For the arc-welded specimens, the MIG welding procedure is applied, without pre-heating, using filler wire 5356 and with one pass on each side. It has to be mentioned that the weld reinforcement is not removed, which may introduce (limited, ignored) 3D effects. The constant amplitude tests at a stress ratio $R_s = 0.1$ [-] and a frequency $f = 10$ [Hz] have been conducted in air. The original results contain some region I as well as region II behavior, as shown in (Figs. 15, 17 and 19).

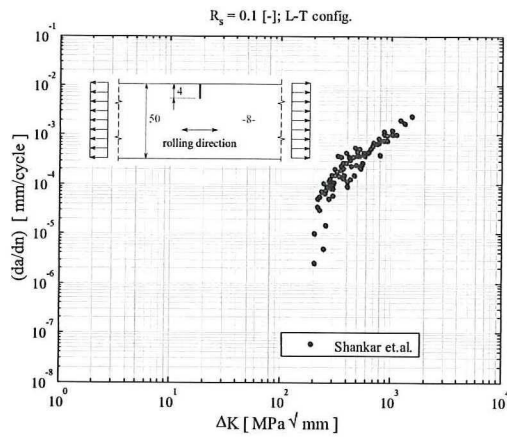


Fig. 15: $(da/dn) - \Delta K$ data of Aluminum 5083-H321 Plain Material (Shankar, 2002)

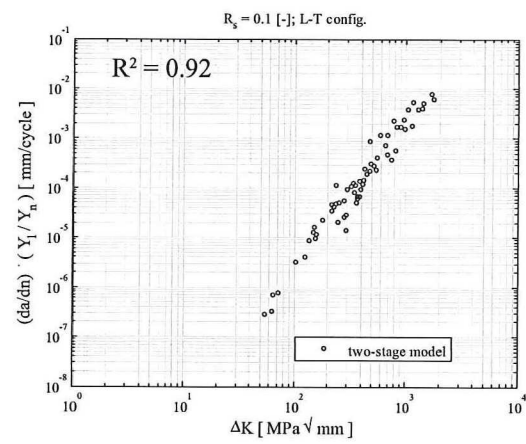


Fig. 18: $(da/dn) - \Delta K$ data of Aluminum 5083-H321, HAZ Crack Growth in Welding Dir., Two-Stage Model

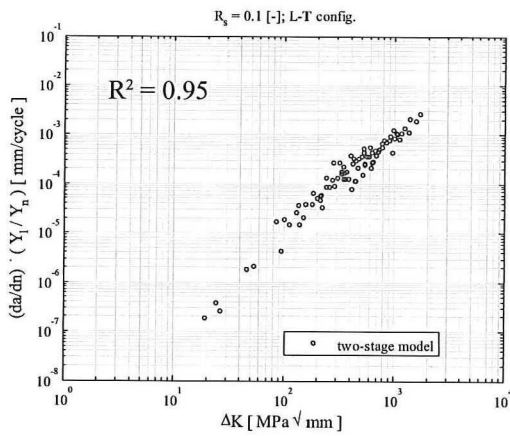


Fig. 16: $(da/dn) - \Delta K$ data of Aluminum 5083-H321 Plain Material, Two-Stage Model

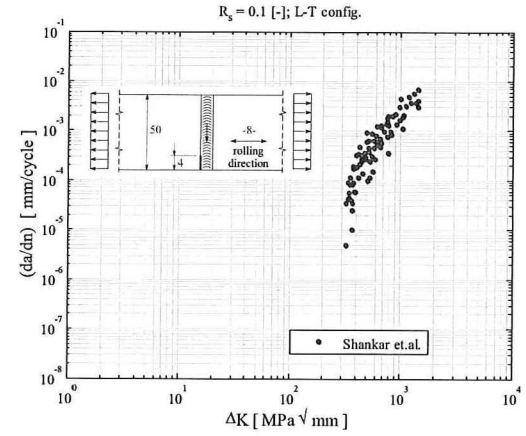


Fig. 19: $(da/dn) - \Delta K$ data of Aluminum 5083-H321, HAZ Crack Growth in Counter Welding Dir. (Shankar, 2002)

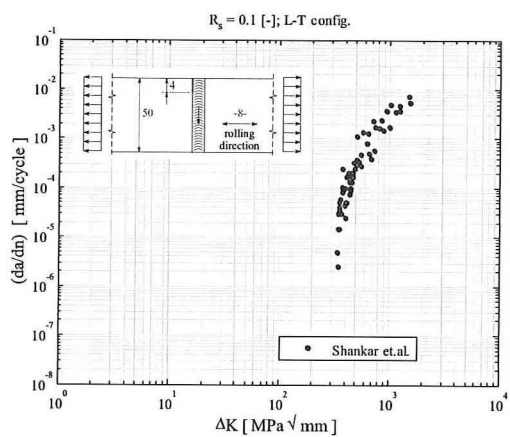


Fig. 17: $(da/dn) - \Delta K$ data of Aluminum 5083-H321, HAZ Crack Growth in Welding Direction (Shankar, 2002)

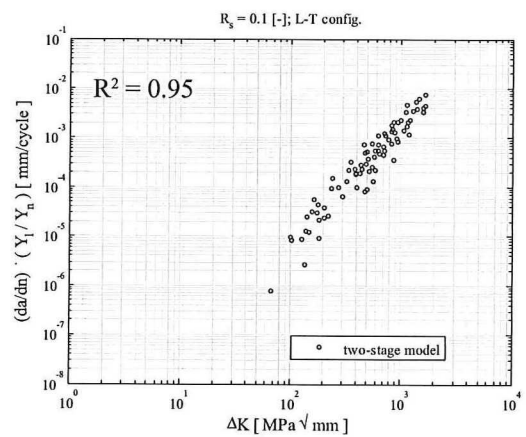


Fig. 20: $(da/dn) - \Delta K$ data of Aluminum 5083-H321, HAZ Crack Growth in Counter Welding Dir., Two-Stage Model

The corresponding results using the two-stage crack growth model are shown in (Figs. 16, 18 and 20). Note that for the calculation, the pre-crack length – about 2 [mm] in this case – has to be included in the initial crack length a_i . The factor $(Y_n/Y_1)^n$ is moved to the left-hand side of (Eq. 18), as shown on the vertical axis title. The remaining part is the single-slope, region II term $C \cdot (\Delta K_g)^m$.

Comparing the original and modified data, it turns out that a small shift in horizontal direction exists: a result of the differences in far field stress definition.

The crack growth data analysis is only intended to show the applicability of the proposed two-stage crack growth model. The material constants C and m will be determined using experimental fatigue test data of aluminum welded joints.

In general, the crack growth behavior in welding direction as well as counter welding direction is more or less similar: consider the slope m . Comparing crack growth in plain material and the HAZ of the DS FP butt weld joints demonstrates that welding changes material properties, as expected. Welding induced residual stresses are included.

Note that for crack growth in plain material as well as in the HAZ of the welded joints, two different materials, the exponent $n = 1$. This exponent is supposed to be a material parameter. However, for the two different materials, n is the same. Actually, this makes sense.

(Dong, 2003b) investigated micro-crack growth for steel as well as some aluminum specimens. Fitting experimental data ended up with $n = 2$, similar for both materials. It is explained by the suggestion that the plastic zone size still dominates micro-crack growth, because the plastic zone size r_y is proportional to K_1^2 : $\{2 \cdot \pi \cdot r_y = (K_1/\sigma_y)^2\}$. Although, another suggestion might be that micro-crack growth (also) can be considered as a pure geometry and loading induced phenomenon, as already shown in (Fig. 1). The governing parameter in the micro-crack growth region is the SCF, indeed, a geometry and loading related parameter. Besides, this suggestion is in agreement with the Notch Stress Intensity (NSIF) approach, introduced by (Atzori, 2008 and Lazzarin et al., 1998). The NSIF is a notch stress based parameter, a geometry parameter, comparable to Y_m and (Y_n/Y_1) up to some extent, to cover the crack initiation period. In short: the micro-crack (growth) behavior, region I behavior, can (also) be considered as a geometry property: $n = 1$ in the proposed two-stage crack growth model.

Conclusions

Analytical, parametric formulations for notch stress distributions have been formulated which covers different types of joints. All geometry parameters are (implicitly) included as variables, to allow studying the influence of structural detail modifications on the fatigue life.

The SIF of a crack at the weld is obtained as a product of crack size dependent correction factors $Y_m(a/t_b)$ and $Y_g(a/t_b)$ and the SIF for the basic case. The geometry factor Y_g , related to the equilibrating stress part, the far field stress, is directly obtained from handbook solutions and covers macro-crack growth. The self-equilibrating stress part, the crack face pressure, is translated to a magnification factor Y_m that covers micro-crack growth. Formulations are analytical and parametric. Results for FP DS T-joints and FP cruciform joints are compared to FE solutions from literature and match quite well.

A two-stage, Paris' equation based, crack growth model is proposed, since a non-negligible part of the fatigue life may be consumed in the micro-crack growth region, region I, because of the low crack growth rate. Promising results are obtained in comparison with experimental crack growth data of a SEN specimen. It has been found that micro-crack growth (also) can be considered as a geometry and loading induced phenomenon.

Acknowledgement

The authors would like to thank the project participants: Damen Shipyards, research institutes MARIN and TNO, classification societies Bureau Veritas and Lloyds Register and the US Coast Guard for funding this research. In addition, the authors are grateful to K. Shankar for providing the experimental crack growth data.

References

- Albrecht P., Yamada K. (1977). "Rapid Calculation of Stress Intensity Factors", Journal of the Structural Division 103, American Society of Civil Engineers (ASCE), pp 377-389.
- Atzori B., Lazzarin P., Tovo R. (1997). "Stress Distributions for V-shaped Notches Under Tensile and bending Loads", Fatigue & Fracture of Engineering Materials, Vol. 20, No. 8, pp 1083-1092.